[논 문] 한국재료학회지
Korean Journal of Materials Research
Vol. 12, No. 1 (2002)

레이저 가공시 에너지 전달과 Plume 효과

강 계 명† · 김 광 열*
서울산업대학교 재료공학과
*삼성전자 책임연구원

Laser-Plume Effects on Radiation Energy Transfer in Materials Processing

Kae Myung Kang† and Kwang Ryul Kim*
Professor, Dept. Materials Science & Engineering, Seoul National Univ. of Technology 172 Gongreung 2-Dong, Nowon-Gu, Seoul 139-743
**Senior Research Engineer, Samsung Electronics Co. Ltd. 416, Maetan-3Dong, Paldal-Gu, Suwon City, Kyungki-Do 442-742*

(2001년 12월 7일 받음, 2001년 12월 28일 최종수정본 받음)

Abstract In laser materials processing, localized heating, melting and evaporation caused by focused laser radiation forms a vapor on the material surface. The plume is generally an unstable entity, fluctuating according to its own dynamics. The beam is refracted and absorbed as it traverses the plume, thus modifying its power density on the surface of the condensed phases. This modifies material evaporation and optical properties of the plume. A laser-produced plasma plume simulation is completed using axisymmetric, high-temperature gas dynamic model including the laser radiation power absorption, refraction, and reflection. The physical properties and velocity profiles are verified using the published experimental and numerical results. The simulation results provide the effect of plasma plume fluctuations on the laser power density and quantitative beam radius changes on the material surface. It is proved that beam absorption, reflection and defocusing effects through the plume are essential to obtain appropriate mathematical simulation results. It is also found that absorption of the beam in the plume has much less direct effect on the beam power density at the material surface than defocusing does and helium gas is more efficient in reducing the beam refraction and absorption effect compared to argon gas for common laser materials processing.

Key words: laser radiation, plasma plume, laser materials processing

I. Introduction

In many laser materials processes, a constant-wave (CW) laser beam is focused onto the material surface at an energy density sufficient to cause localized heating and evaporation. As a result, a plume of hot, excited and ionized material vapor and ambient gas forms above the surface. Examples of CW laser processes where plume formation is important include cutting and joining. Measurements of the portion of the plume visible above the work surface during laser welding generally yield temperatures from 5200 K to 13,000 K and electron densities are the order of 10^{15} to 10^{17} cm^{-3}, depending on the substrate material, ambient atmosphere and laser power.[1~3] Partially ionized gases absorb infrared wavelength by the inverse Bremsstrahung mechanism.[4] In addition, electron density plays an important role in determining the refractive properties of the plume, so electron density gradients in the plume lead to defocusing of the beam. The power and focusing trajectory of the laser beam are modified as it traverses the partially ionized plume, modifying the laser power density impinging on the condensed phases of the material. However, since power density on the material affects plume temperature, ionization and other properties, there exists the potential for significant coupling between the plume, beam propagation and the material response. This coupling is so strong that it was recently exploited to create a self-modulating laser joining process, where dynamic fluctuations in the plume arising due to coupling were used to self-pulse the beam power density at the work surface.[5] Optimization of this and other laser materials processes requires that beam-plume interactions be considered.

† E-mail: littbird@duck.snut.ac.kr

Although a large amount of past work dealing with the plume formation in laser materials processing has been reported, detailed dynamic models for analyzing effects in the portion of the plume above the material surface to the extent that they are dealt with in this work have not been previously available. This work is most closely related to the earlier work of Beck et *al.*[6] who calculated absorption and defocusing of a laser beam propagating through a laser-induced plasma with assumed composition and temperature distributions. Although the assumed plume models were approximate, the work concluded that both absorption and refraction have significant effects on the power density at the work surface. This work extends those previous results by incorporating laser beam propagation into a relatively complete physical model of the plume so that the interaction of the two is studied in detail. An example of earlier models of pulsed laser plumes evolving from condensed phase surfaces is one described by Aden, Beyer and Herziger.[7] In this and much of the earlier work, plume and beam interactions were not considered. More recently, models of CW laser-induced plumes within deep keyholes that include laser and plume interaction have been the subjects of numerous articles.[8~11] The present work is concerned with CW laser plumes above material surfaces. Many articles[12~14] and a book15 provide examples of recent models of pulsed laser material plumes, which is similar in some respects. The laser energy absorption is sometimes considered in these analyses but not the beam propagation. An approximate analytical model of a CW laser plume formed over a material surface that incorporates beam propagation is discussed by Dowden, Kapadia and Ducharme.[16]

In this paper, a coupled dynamic model of the plume, beam propagation and material to understand the plasma plume dynamics and calculate the beam intensity changes on the material surface during CW CO_2 laser welding is presented. In addition, the results of the beam radius changes on the material surface for various plume interaction are compared and analyzed. Finally, the results of time variation of beam irradiance on the material surface for various plume interaction are presented and explained.

2. Axisymmetric model of laser-produced plasma plume

The laser beam propagation is assumed to be axisymmetric and Gaussian. To save computing time, the material surface is assumed to be an adiabatic.

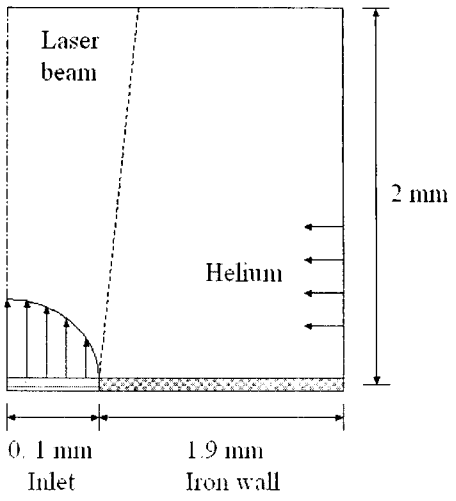

Fig. 1. Initial and boundary conditions for plume simulation

The initial velocity fields are assumed to be Gaussian and no-slip condition at the wall. To simulate the shielding gas effect, uniform flows of helium or argon gases (5-10 m/sec) are assumed from the side boundary to the plasma plume center. It is assumed that the beam absorption into the material is 13 %[22] and the beam reflection into vapor is 50 %.[2] The initial and boundary conditions are shown in figure 1.

The compressible Navier-Stokes equations in the axisymmetric cylindrical coordinate system can be written as[17]

$$\frac{\partial \rho}{\partial t}+\frac{1}{r}\frac{\partial}{\partial r}(\rho r u_r)+\frac{\partial}{\partial z}(\rho u_z)=0 \tag{1}$$

$$\frac{\partial}{\partial t}(\rho u_r)+\frac{1}{r}\frac{\partial}{\partial r}(\rho r u_r^2)+\frac{\partial}{\partial z}(\rho u_r u_z)+\frac{\partial p}{\partial r} -\frac{1}{r}\frac{\partial}{\partial r}(r\tau_{rr})+\frac{\tau_{\theta\theta}}{r}-\frac{\partial}{\partial z}(\tau_{rz})=0 \tag{2}$$

$$\frac{\partial}{\partial t}(\rho u_z)+\frac{1}{r}\frac{\partial}{\partial r}(\rho r u_r u_z)+\frac{\partial}{\partial z}(\rho u_z^2)+\frac{\partial p}{\partial z} -\frac{1}{r}\frac{\partial}{\partial r}(r\tau_{rz})-\frac{\partial}{\partial z}(\tau_{zz})+\rho g=0 \tag{3}$$

$$\frac{\partial E_t}{\partial t}+\frac{1}{r}(r u_r E_t)+\frac{\partial}{\partial z}(u_z E_t)+\frac{\partial}{\partial r}(\rho u_r) +\frac{\partial}{\partial z}(\rho u_z)+\frac{1}{r}\frac{\partial}{\partial r}(r q_r)+\frac{\partial}{\partial z}(q_z) -\frac{1}{r}\frac{\partial}{\partial r}(r u_r\tau_{rr}+r u_z\tau_{rz})-\frac{\partial}{\partial z}(u_r\tau_{rz}+u_z\tau_{zz}) +\frac{u_r}{r}(\tau_{\theta\theta})-\sum aI=0 \tag{4}$$

where

$$\tau_{rr}=\frac{2}{3}\mu\left[2\frac{\partial u_r}{\partial r}-\frac{\partial u_z}{\partial z}-\frac{u_r}{r}\right],\quad \tau_{\theta\theta}=\frac{2}{3}\mu\left[\frac{u_r}{r}-\frac{\partial u_r}{\partial r}-\frac{\partial u_z}{\partial z}\right]$$

$$\tau_{zz}=\frac{2}{3}\mu\left[2\frac{\partial u_z}{\partial z}-\frac{\partial u_r}{\partial r}-\frac{u_r}{r}\right],\ \tau_{rz}=\tau_{zr}=\mu\left(\frac{\partial u_r}{\partial z}+\frac{\partial u_z}{\partial r}\right)$$

$$q_r=-k\frac{\partial T}{\partial r},\ q_z=-k\frac{\partial T}{\partial z},\ \frac{dI}{dz}=-\alpha I,\ E_t=\rho\left(e+\frac{u_r^2+u_z^2}{2}\right)$$

In the equations (1) through (4), the term u_r is the velocity along r direction, u_z is velocity along z direction, ρ is the density, p is the pressure, T is the temperature, k is the thermal conductivity, I is the local laser intensity including reflection from material melting surface, α is the absorption coefficient, μ is the viscosity, g is the gravitational constant, and e is the internal energy.

Flow in the plume model is induced by atomic vapor evolving from the material surface. In a thin (several mean free paths-thick) region at the surface known as the Knudsen layer, the thermal motion of the vapor particles is considered to change from a half-Maxwellian distribution to a full-Maxwellian distribution characteristic of a free gas.[18] By a kinetic analysis of the Knudsen layer flow, the state of the vapor on the downstream side of the layer can be expressed in terms of the surface temperature, T_V, of the liquid and the Mach number of the vapor flow on the downstream side of the layer.[7] These relations, which are used to calculate inlet conditions for the plume simulation, are

$$T_{v,\,inlet}\cong(1-0.33M_1)\,T_v \tag{5}$$

$$\rho_{v,\,inlet}\cong\overline{\rho}\,(T_v)/(1+0.22M_1) \tag{6}$$

where the overbar refers to properties of vapor in equilibrium with the liquid (saturated vapor) at the vapor-liquid boundary of the base material. The term M_1 is Mach number. The subscripts "v" and "inlet" represent vapor and inlet quantities, respectively. Making common assumption[7] that steady vapor flow approaches sonic speed at the inlet, we can use following equations to obtain the inlet conditions for the vapor simulation in terms of the surface temperature of the liquids

$$T=0.67\overline{T} \tag{7}$$

$$\rho=0.31\overline{\rho} \tag{8}$$

$$P=0.21\overline{P} \tag{9}$$

It is necessary to calculate the pressure of vapor in equilibrium with the liquid surface to obtain vapor density across the Knudsen layer. One can calculate equilibrium vapor pressure as a function of temperature by integrating the Clausius-Clapeyron relation, resulting in the expression[19],

$$\overline{p}(T_v)=p_0\exp\left[\Delta H_{lv}\frac{T_v-T_{lv}}{RT_vT_{lv}}\right] \tag{10}$$

where T_{lv} is the liquid-vapor equilibrium temperature at atmospheric pressure p_0, R is the universal gas constant, and the term ΔH_{lv} is the molar latent heat of liquid-vapor. A perfect gas relation is then used to obtain the saturated vapor density

$$\overline{\rho}\,(T_v)=\overline{\rho}\,(T_v)\,M/RT_v \tag{11}$$

where M is the atomic mass. The Mach number of the vapor is the ratio of its calculated speed to the theoretical sound speed $V_{s,\ inlet}$ at the downstream side of the Knudsen layer[19]

$$M_1=V_{v,\ inlet}/\sqrt{\gamma\frac{p_{v,\,inlet}}{\rho_{v,\,inlet}}} \tag{12}$$

where γ is the ratio of specific heats. If the temperature on the steel surface (liquid-vapor boundary) is 3520 K and the flow speed is Mach 1, we obtain 2288 K for the inlet vapor temperature. The Sutherlands law is widely used to determine the viscosity of dilute gases.[17] However, the Wilkes formula[20] is applied to this simulation, since it is more convenient for the variety of gas mixtures simulations without searching the Sutherlands constants. The thermal conductivity of pure atomic species i is calculated from the Chapman-Enskog relation. The heat capacities of the individual components, including the effects of single ionization, are calculated from[21]

$$C_v=\frac{3}{2}R(1+\alpha_I)+R\alpha_I\frac{1-\alpha_I}{2-\alpha_I}\left(\frac{3}{2}+\frac{\theta_I}{T}\right)^2 \tag{13}$$

$$C_p=\frac{5}{2}R(1+\alpha_I)+\frac{R\alpha_I}{2}(1-\alpha_I^2)\left(\frac{5}{2}+\frac{\theta_I}{T}\right)^2 \tag{14}$$

where $\theta_I=V_Ie N_0/R$ and α_I denotes the degree of ionization. In the above equations, V_I is the ionization potential, e is the electron charge, N_0 is the Avogadros number, R and is the universal gas constant. It is assumed in this work that the ionization can be calculated from the Saha equation (since local thermal equilibrium conditions apply in the laser plume at atmospheric pressures), coupled with a perfect gas equation of state, both written for single ionization as[21]

$$\frac{n_s^+n_e}{n_s}=\frac{2Z_x^+}{Z_s}\frac{(2\pi m_e kt_e)^{3/2}}{h^3}\exp\left(-\frac{eV_{I,s}}{k_bT_e}\right) \tag{15}$$

$$p=(n_e+n_{he}+n_{fe}+n^+{}_{he}+n^+{}_{fe})\,k_bT_e \tag{16}$$

Table 1. Physical properties for vapor simulation

Input Variables	Values	Units
Vaporization temperature of Iron	3135.0	K
Atmospheric pressure	101325.0	Pa
Universal gas constant	8.314	J/mol K
Molar mass of Iron	55.8×10^{-3}	Kg/mole
Molar mass of Helium	4.003×10^{-3}	Kg/mole
Inlet diameter	0.00021	m
Ionization potential of Fe	7.9	V
Ionization potential of He	24.58	V
Saha Equation		
Partition function of Fe (Zfe)	43	-
Partition function of Fe ion (Zfe+)	57	-
Partition function of He (Zhe)	1	-
Partition function of He ion (Zhe+)	2	-
Boltzmann Constant	1.38×10^{-23}	J/K
Laser Power	3000	W

where n is the particle density, Z_s is the partition function of the component, h is the Plank constant, k is the thermal conductivity, m_e is the mass of electron, k_b is the Boltzmann constant, the superscript "+" denotes positive ion and the subscripts "*fe*" and "*he*" represent iron and helium respectively. The absorption coefficient for CO_2 laser radiation was calculated assuming that inverse Bremstrahlung is the dominant mechanism[21]

$$\alpha = 3.3\times10^{-39}\frac{n_e^2}{T_e^{3/2}} \tag{17}$$

where n_e is the electron particle density and T_e is the electron temperature. The physical properties used in the plume simulation are summarized in table 1.

The initial conditions at the inlet calculated from the result of the material model.[22] All physical properties at the inlet are updated at each time step as a result of the consideration of the beam absorption, refraction and reflection at the material surface. The axisymmetric boundary conditions are applied for all physical properties along the symmetric line. The physical domain size along the z direction can be changed as a result of the transient behavior of the plume vapor under certain conditions. Boundary conditions at the outlet are calculated by extrapolation technique. The explicit MacCormack scheme is used to calculate velocity, density and temperature profiles in the plasma plume. The optimal time step for calculation is determined by considering the Von Neumann stability analysis and Courant-Friedrichs-Levy (CFL) conditions at each time step. The helium and iron vapor mixing is computed using continuity equations of each components. The continuity equations are combined with the Navier-Stokes equations and computed at the same time step.

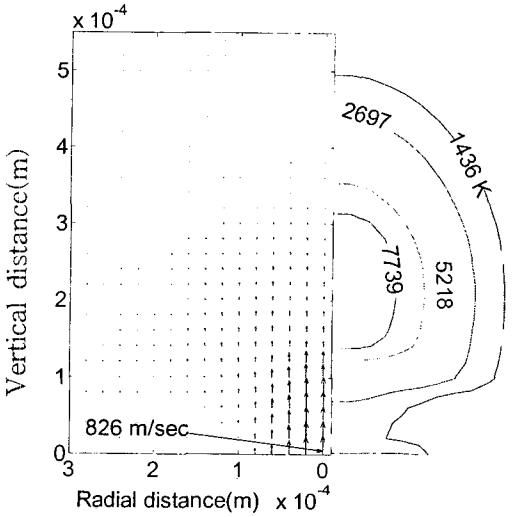

Fig. 2. Velocity (m/sec) and temperature(K) profiles at 10^{-9} sec Inlet maximum velocity is 826 m/sec

The Gaussian velocity distribution at the inlet can be written as[23]

$$U_z = U_{z0}\exp\left[-\frac{2r^2}{ir^2}\right] \tag{18}$$

where ir is the inlet radius U_{z0} is the sonic speed based on the inlet temperature.

The initial conditions (at 10^{-9} sec) of the pressure contours and velocity fields are shown in figure 2. The initial plasma plume is assumed to be the elliptical shape and Gaussian temperature distribution as shown below[6]

$$T(r,z) = T_{M,\max}\exp\left[-2\left(\frac{r^2}{r_M^2}+\frac{(z-h_M)^2}{z_M^2}\right)\right] \tag{19}$$

where $T_{M,max}$ is the maximum temperature in the center of the plasma plume, r_M is the half axis width of the plasma plume, Z_M is the half axis length of the plasma plume and h_M, is the height of the plasma plume center above the surface of the material surface. The initial condition (at 10^{-9} sec) of the temperature field is shown in figure 2.

Introducing the complex index of refraction and complex scalar wave amplitude, the wave equation can be written in paraxial form[6]

$$2ik\frac{\partial U}{\partial z}=\nabla^2 U+k^2(\hat{n}^2-1)\,U \qquad (20)$$

where $k=\frac{2\pi}{\lambda}$, $\hat{n}=\left[\frac{\omega_e\omega_p^2}{\omega(\omega_p^2+\omega_e^2)}\right]i$

$\omega=\frac{c}{\lambda}$, $\omega_p=\sqrt{\frac{e_0^2 n_e}{\varepsilon_0 m_e}}$

In above equations, the term k is the propagation constant, $\hat{n}$ is the complex index of refraction, ω is the laser frequency, ω_p is the plasma laser frequency, ω_e is the electron collision frequency, e_0 is the elementary charge, n_e is the electron number density, ε_0 is the permittivity of vacuum, m_e is the electron mass, c is the speed of light, λ is the laser wavelength, and U is the phasor amplitude representing the transverse profile.

Considering Hamilton factor, we can represent the paraxial wave equation as follows:

$$\frac{\partial U}{\partial z}=-iHU \qquad (21)$$

where the Hamilton factor H is:

$$H=\frac{1}{2k}\left[\frac{\partial^2}{\partial r^2}+\frac{1}{r}\frac{\partial}{\partial r}+k^2(\hat{n}^2-1)\right]$$

Gaussian beam intensity can be written as[23]

$$I(r,z)=\frac{2P}{\pi w^2(z)}\exp\left[\frac{-2r^2}{w(z)}\right] \qquad (22)$$

where $P=\frac{1}{2}I_0(\pi w_0^2)$, r is the radius, I_0 is the overall peak intensity, and $w(z)$ is the transverse beam radius.

3. Verification of the plasma model simulation

Since the plasma plume is so hot and bright, it is very difficult to visualize the velocity field or measure the velocity from experiments. Since no experimental results have been reported yet, we present other previous theoretical and numerical results and compare our data with theirs.

After going throug the Knudsen layer, the vapor velocity becomes the local sonic speed.[24] This initial velocity is accelerated under high temperature conditions and

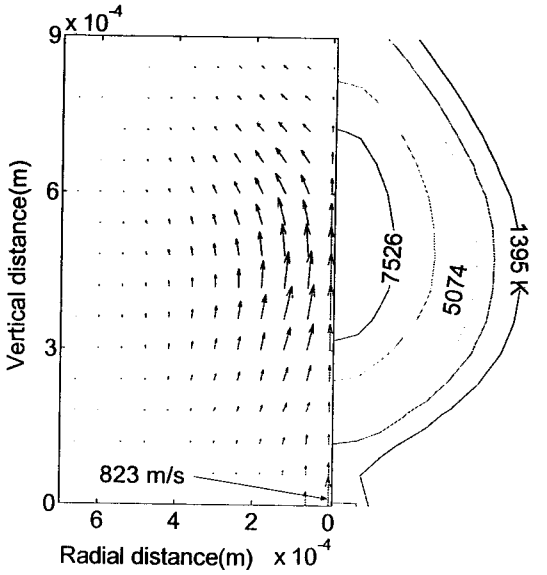

Fig. 3. Velocity (m/sec) and temperature (K) profiles at 5×10^{-1} sec, helium

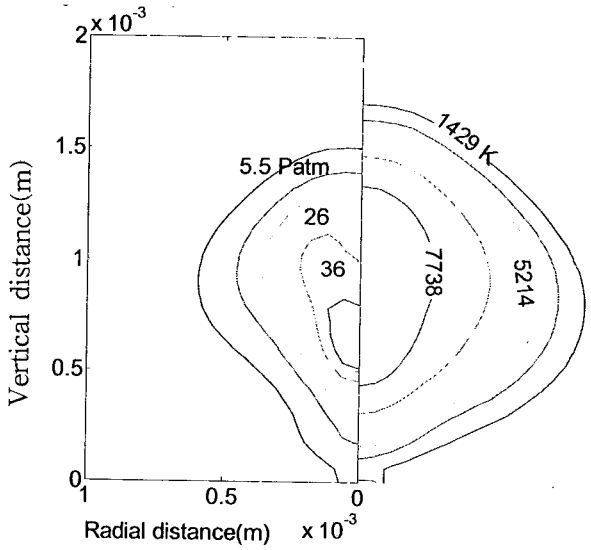

Fig. 4. Pressure contours (Patm) and temperatures (K) at 10^{-5} sec, helium

decelerated at the vapor front. Aden et *al.*[7] solved the Euler equations, the steady heat-flow equation, and the kinetic equation to calculate the gas dynamic properties at the edge of the Knudsesn layer. They computed the velocity of the metal vapor and the displaced ambient air for an absorbed laser intensity of 10^{10} W/m^2. They also calculated the velocity of the metal vapor and the displaced ambient air for an absorbed laser intensity of 10^{10} W/m^2. At the intensity of 10^{11} W/m^2, the pressure is increased up to 60 P_{atm} and decreased down to 25 h P_{atm}. The inlet velocity, maximum velocity, and maximum pressure in figures 3 and 4 are compatible with those found in the Adens

model. In figure 3 and 4, the laser power 3KW is used on the 0.21 mm spot size.

Poueyo *et al.*[25] measured averaged plasma temperature of 5200-6800 K using the spectroscopic method, when welding iron plates $1\times10^{10}\sim5\times10^{10}$ W/m^2 power density under helium shielding gas. Sokolowski[26] reported averaged 7500 K plasma temperatures under a power density of 4×10^{10} W/m^2. He used helium as a shielding gas. Poueyo *et al.*[2] again measured the electron temperature of 6300 6900 K using 1 and 15 kW laser power with helium shielding gas. The maximum plasma plume temperature at simulation time of 10^{-5} seconds (figure 4) is 8100 K. The helium is used for shielding gas. The axisymmetric simulations are well verified through previous numerical and experimental results.

4. Results of numerical simulations

Since the plasma plume interacts with the propagating laser beam during laser materials processing, the absorption effect is one of the most important process parameters. Considering the zero absorption case, the initial maximum temperature decreases very fast with time. The steady state vapor is eventually established based on inlet temperature that is result from the material surface evaporation. The plume is cool and it does not affect the plume. If there is no absorption through plume vapor, the surface power intensity is always constant. In contrast, the surface power intensity is increased or decreased based on the plume dynamics and plasma plume evolution. The temperature profile and pressure contours

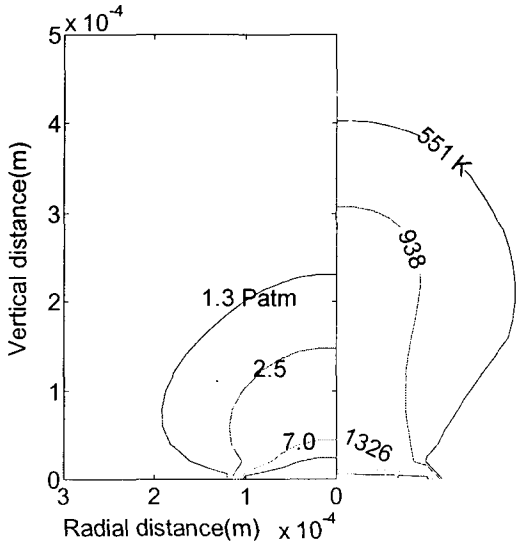

Fig. 5. Pressure (Patm) contours and temperature (K) profiles at 5×10^{-6} sec, Zero absorption

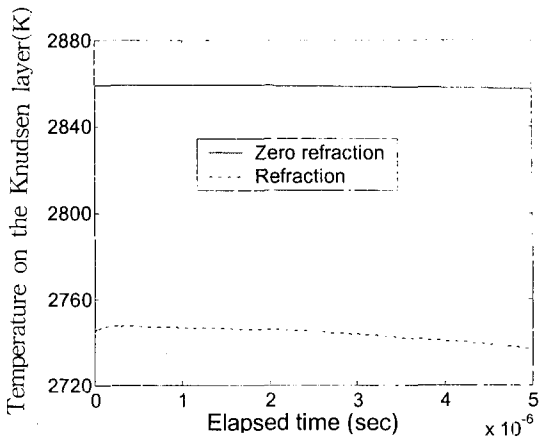

Fig. 6. Temperature changes on the Knudsen layer

of the zero absorption case at the time of 510^{-6} seconds is shown in figure 5. Compared with the zero absorption case, the absorption case shows dramatically different results. The plasma vapor seems to be stabilized during certain initial time periods with somewhat lower temperature (about 7000 K) and continuously expands as a result of the beam absorption until it meets the critical point that the vapor detaches from the material surface. After this time, the maximum temperature is reached at 8100 K. The vapor size is decreased slowly and disappears completely. Since the propagating laser beam is refracted through the high temperature plasma plume, its radius is changing. The results of velocity and temperature profile are presented in figures 3. Turning off the effect of refraction, we obtained almost same result with refraction case. Therefore it is found that if the helium gas is the predominant composition of the plasma plume, the defocusing effect is almost negligible to affect physical properties in the plume. The more evolved transient helium gas case is shown in figure 4. The pressures are increased until 36 atmospheric pressure and temperatures are increased up to 8100 K in core region. The vapor size is about 2 mm heights. Comparing the vapor temperature changes on the Knudsen layer in figure 6, we found that there is a 120 K surface temperature difference between zero refraction and refraction case. Since their vapor size, temperature profiles and absorption coefficients are almost same, we induce that the refraction effect makes that much temperature difference. Therefore it is concluded that the refraction has important effect on surface intensity rather than absorption. This will be discussed in detail at the end of this section.

The shielding gas is one of the very important parameters in laser materials processing to achieve high quality manufacturing results. The helium and argon are

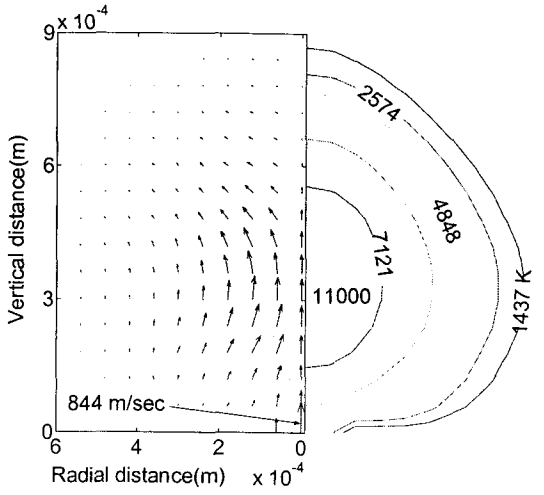

Fig. 7. Velocity (m/sec) and temperature (K) profiles at 5×10^{-6} sec, argon

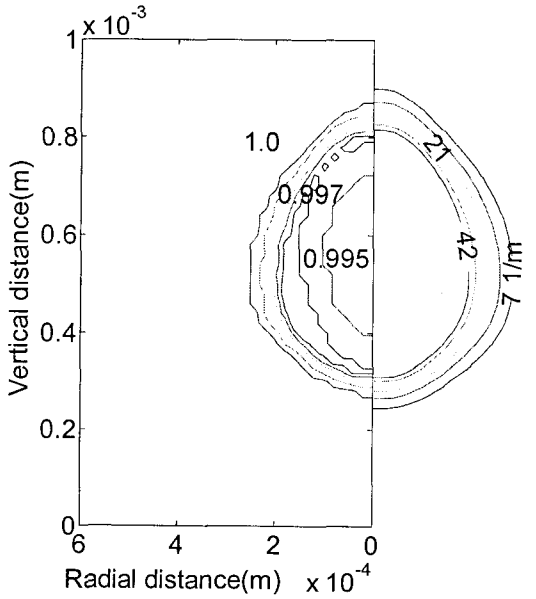

Fig. 8. Index of refraction and absorption coefficients (1/m) at 5×10^{-6} sec, helium

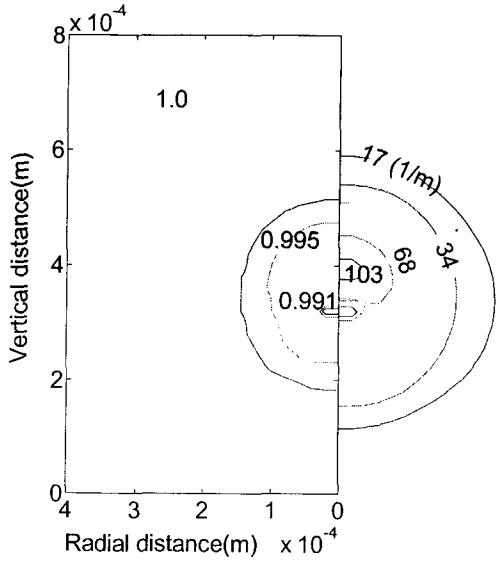

Fig. 9. Index of refraction and absorption coefficients (1/m) at 5×10^{-6} 5×10^{-6} sec, agron

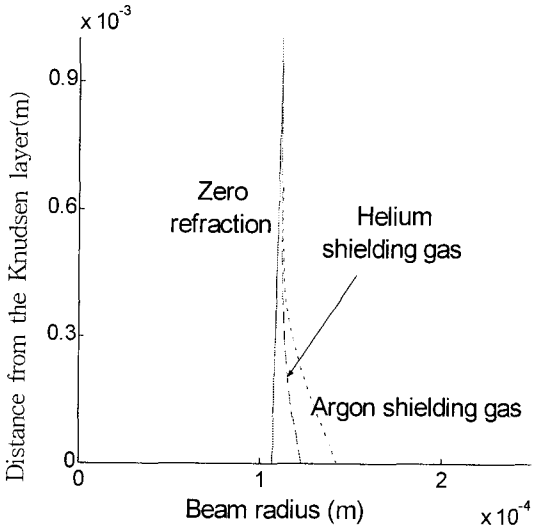

Fig. 10. Beam radius changes based on the shielding gases at 5×10^{-6} sec

very popular shielding gases in laser materials processing for common manufacturing purposes. The laser material interaction under argon shielding gas is presented in figure 7. It shows that the maximum temperature is higher compare with helium case. In addition, the averaged plasma temperature is also higher than one of the helium shielding gas case. Comparing the inlet velocity from helium case at the same time, we find that that the flow velocities are faster in argon case.

The location of the plasma plume (depending on time and intensity in laser material processing) is very important, because the evolved plasma plume can absorb and refract the propagating laser beam and deliver lower beam intensity on the material surface. During laser welding, the plasma plume appears to evolve from the inside of the keyhole into the ambient atmosphere. Seidel *et al.*[27] investigated that the plasma plume remains attached at the entrance of the keyhole at relatively low laser intensity. This attached steady plasma is not important in propagating incident laser radiation.[27] At high laser intensities, the plasma plume evolves from the keyhole and expanded plasma interrupts and refracts the propagating laser beam. This causes separation of the plasma from the material surface. In figures 8, the results of the real part of the index of refraction as well as absorption coefficients are shown. Since the laser beam propagation is disturbed by index of refraction, it becomes very important variables to figure out the beam defocusing effect in the plasma plume. The real part of the index

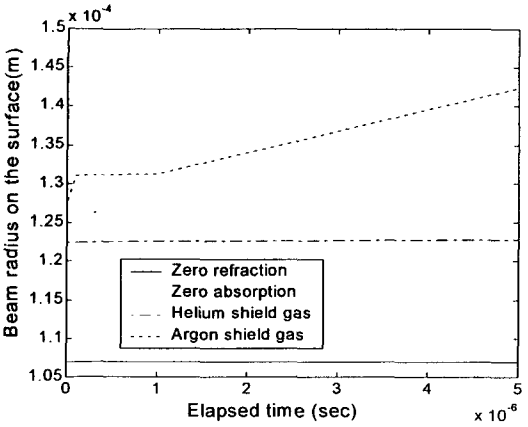

Fig. 11. Beam radius changes on the material surface for various plume interaction and ambient atmosphere conditions.

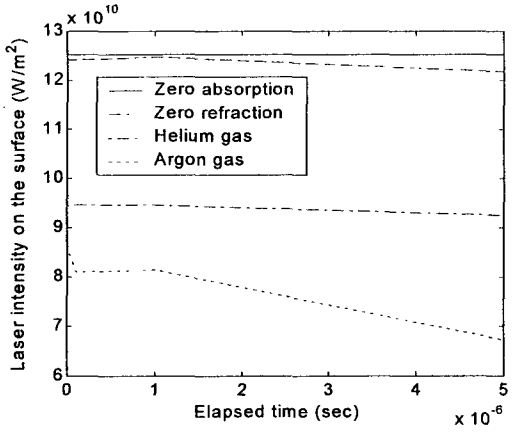

Fig. 12. Time variation of beam irradiance on the material surface for various plume interaction and ambient atmosphere conditions

of refraction is decreased down to 0.995 and absorption coefficient is increased up to 42 (1/m) near the maximum temperature region. The results of argon case are shown in figure 9. Because of higher temperature near the plasma center region, the value of the real part of the index of refraction is somewhat smaller and the value of the absorption coefficients is bigger than helium case. The real part of the index of refraction of argon is decreased down to 0.991and absorption coefficient is increased up to 103 (1/m) near the plasma plume center. The smaller real part of index of refraction is appears, the bigger beam defocusing effects. In figure 10, the propagating beam radius changes based on the two different shielding gases are presented. It is obvious that the laser beam is defocused as it propagates through the plume. The beam radius changes on the material surface for zero refraction, zero absorption, helium shield gas, and argon shield gas cases are shown in figure 11. In the cases of zero refraction and zero absorption, the beam radius does not change during the simulation. At the simulation time 5 $\times 10^{-6}$ sec, the beam radius for helium shield case is increased by 15 %. Since high absorption coefficients and refraction, the beam radius for argon case is increased by 33 %. The beam irradiance changes on the material surface for above four cases are shown if figure 12. The beam intensity is decreased by 26 % due to absorption and refraction effects in helium shielding gas. For argon shielding gas, the beam intensity can be decreased by 46 %. Considering the zero refraction case, the beam intensity is only decreases by 3 % due to the absorption effect. Consequently, it is found that the beam radius is highly increased by refraction effects and absorption has small effect on the beam intensity on the material surface.

5. Conclusions

An axisymmetric laser-produced plasma plume model is presented and obtained following conclusions.

1) The beam absorption is essential for plume formation.

2) The laser beam is defocused as it propagates through the plasma plume.

3) Refraction of the propagating CO_2 laser beam in the plasma plume has much bigger effect on the beam power density into the material than absorption does.

4) Beam power density changes that result as the plume evolves significantly affect the properties of the vapor entering the plume.

5) Refraction has important effect on surface intensity, but little effect on plume properties.

6) Helium gas is very efficient in reducing the beam refraction and absorption effect for high quality laser materials processing compared to argon gas.

Consequently, the large plume variations in CO_2 laser welding is a factor in overall process dynamics.

Acknowledgement

This work was supported by the research fund of Seoul National University of Technology.

References

1. W.W. Duley, Laser welding, (John Wiley & Sons, Inc., New York, 1998).
2. A. Poueyo-Verwaerde, R. Fabbro, G. Deshors, A.M. de Frutos and J.M. Orza, J. Appl. Phys. 74, 5773 (1993).
3. Z. Szymanski and J. Kurzyna, J. Appl. Phys., 76, 7750 (1994).
4. T.P. Hughes, Plasmas and Laser Light, (Wiley, New York, 1975), pp. 39-47.

5. A. Matsunawa, N. Seto, M. Mizutani, S. Katayama, IIW Doc. IV-753-99 (1999).
6. M. Beck, P. Berger, H. Hügel, J. Phys. D: Appl. Phys., **28**, 2430 (1995).
7. M. Aden, E. Beyer and G. Herziger, J. Phys. D: Appl. Phys. **23**, 655 (1990).
8. A. Kaplan, J. Phys. D: Appl. Phys., **27**, 18051 (1994).
9. A. Kar and J. Mazumder, J. Appl. Phys., **78**, 63 (1995).
10. C. Tix, U. Gratzke and G. Simon, J. Appl. Phys., **78**, 6448 (1995).
11. P. Solana, P. Kapadia, J.M. Dowden, P.J. Marsden, J. Phys. D: Appl. Phys., **32**, 942 (1999).
12. A. Kar and J. Mazumder, Physical Review E, **49**, 410 (1994).
13. R. Bellantone, and Y. Hahn, J. Appl. Phys., **76**, 1436 (1994).
14. R. Bellantone, and Y. Hahn, J. Appl. Phys., **76**, 1447 (1994).
15. J.C. Miller and R.F. Haglund, Jr,(eds.), *Laser ablation and desorption,* (Academic Press, San Diego CA, 1998).
16. J. Dowden, P. Kapadia, R. Ducharme, Transport Phen. In Mat. Proc. Mfg., (Colorado Spgs. Conf., 1994).
17. K.A. Hoffmann and S.T. Chiang, *Computational Fluid Dynamics Vols I, II,* (Engineering Education System, Wichita, KS. 1998).
18. C.J. Knight, C. J, AIAA J., **17**, 519 (1979).
19. M. Von Allmen, M. and A. Blatter, Laser-Beam Interactions with Materials, (Springer-Verlag, Berlin Heidelberg, 1995).
20. D.R. Gaskell, An Introduction to Transport Phenomena in Materials Engineering, (MacMillan, New York, 1992).
21. J. Lancaster, Physics of Welding, (Pergamon Press, Oxford, 1986).
22. J. Xie and A. Kar, J. Appl. Physics, **81**, 3015 (1997).
23. B.E.A. Saleh and M.C. Teich, *Fundamentals of photonics,* (John Wiley and Sons, New York, 1991).
24. A. Anisimov and V.A. Khokhlov, *Instabilities in laser-matter interaction,* (CRC Press, Boca Raton, 1995).
25. A. Poueyo, G. Deshors, R. Fabbro, A.M. de Frutos and J.M. Orza, Laser Advanced Materials Processing'92, **1**, 323 (1992).
26. W. Sokolowski, G. Herziger and E. Beyer, Proc. SPIE, **1132**, 228 (1989).
27. B. Seidel, J. Beersiek and E. Beyer, Proc. SPIE **2207**, 279 (1994).